The Spectral Imaging facility: setup characterization

Simone De Angelis,[1,a] Eleonora Ammannito,[1,2] Tatiana Di Iorio,[3] Maria Cristina De Sanctis,[1] Paola Olga Manzari,[1] Fabrizio Liberati,[4] Fabio Tarchi,[5] Michele Dami,[5] Monica Olivieri,[5] Carlo Pompei,[5] Raffaele Mugnuolo,[6]

[1]*Institute for Space Astrophysics and Planetology, INAF-IAPS, Via Fosso del Cavaliere, 100, 00133 Rome, Italy*
[2]*Department of Earth, Planetary and Space Sciences—UCLA, Los Angeles, CA, USA*
[3]*ENEA, UTMEA-TER, Rome, Italy*
[4]*Opto Service SrL, Campagnano di Roma, Italy,*
[5]*Selex ES, Campi Bisenzio (Fi), Italy*
[6]*Italian Space Agency, ASI, Spatial Geodesy Center, Matera, Italy*

The SPIM facility is a laboratory VIS-IR spectrometer developed to support space borne observations of rocky bodies of the Solar System. Currently this laboratory setup is used to support the DAWN mission, which is in its journey towards the asteroid 1-Ceres, and to support the 2018 Exo-Mars mission in the spectral investigation of the Martian subsurface. The main part of this setup is an imaging spectrometer that is a spare of the DAWN Visible InfraRed spectrometer (VIR). The spectrometer has been assembled and calibrated at Selex ES and then installed in the facility developed at the INAF-IAPS laboratory in Rome. The goal of SPIM is to collect data to build spectral libraries for the interpretation of the space borne and in-situ hyperspectral measurements of planetary materials. Given its very high spatial resolution combined with the imaging capability, this instrument can also help in the detailed study of minerals and rocks. In this paper the instrument set-up is first described, and then a series of test measurements, aimed to the characterization of the main subsystems, are reported. In particular laboratory tests have been performed concerning (i) the radiation sources, (ii) the reference targets and (iii) linearity of detector response; the instrumental imaging artifacts have also been investigated.

1. INTRODUCTION

The planetary exploration missions point increasingly both on orbiting and on landing on planetary surfaces, thus not just on collecting remote sensed data but also in-situ chemical and spectroscopic composition data (both on the surface and in the shallow subsurface, e.g. ExoMars 2018 mission). These in-situ analyses will provide high resolution data for the validation of remote sensed data, but in turn need to be validated with measurements on minerals and rocks of similar composition that can be found on Earth and meteorites, by means of facilities that have the same or similar characteristics as those on-board the spacecrafts. Since Visible and near-Infrared reflectance spectroscopy is among the principal techniques for planetary surface mineralogical characterization, the SPectral IMager (SPIM) laboratory set-up has been developed to support remote spectroscopy of Solar System rocky bodies. The core of SPIM is an imaging spectrometer that is a replica of the Visible InfraRed imaging spectrometer (VIR)[1], on-board the DAWN spacecraft. The spectral range of the instrument is 0.2-5.1 µm. The SPIM spectrometer has been assembled and

calibrated at Selex ES and then installed in the INAF-IAPS laboratory in Rome. The SPIM facility is currently used to support the DAWN mission[2] and the 2018 ExoMars mission[3] in the spectral analyses of planetary analogues (minerals, rocks, meteorites). The goal of Dawn mission is to orbit Vesta and Ceres asteroids, in order to collect data that will provide a better understanding of the conditions and processes acting in the early solar system. Thus the SPIM has a key role in characterization of meteorites and terrestrial analogues of planetary materials and to create a spectral database, for validation of remote sensed data. Thanks to powerful and distinctive performances (very high spatial and spectral resolution and imaging capability) this instrument can also be thought as a useful laboratory setup for mineralogical and petrographic characterization.

2. LABORATORY SETUP

The main part of the facility consists of a Visible and Infrared imaging spectrometer that is a spare of the one on-board the DAWN spacecraft[1,4]. Nevertheless the optical layout (fig.1) is different from that of VIR, because in the latter case the observed target is at an infinite distance (a telescope is used in order to focus a parallel beam) while in the former case the observed target is at a finite distance (few centimeters; a divergent beam must be focused).

---
[a]Author to whom correspondence should be addressed. Electronic mail: simone.deangelis@iaps.inaf.it

Moreover in the laboratory facility the sample to be analysed is at room conditions (T=300K and P=1bar) while the spectrometer and the IR detector are cooled and hosted within a Thermo-Vacuum Chamber (TVC, fig.1,3).

Two separate radiation sources are used in order to cover the whole spectral range (0.2-5.1 μm): a Quartz Tungsten Halogen (QTH) lamp is used for the UV-VIS-NIR range (0.2-2.5 μm) and an Infrared Emitter for the IR range (2.5-5.1 μm). The radiations emitted by the two sources are launched in two different set of 7 optical fibres, each transparent in the relevant portion of the spectrum. At the other end, the fibres are arranged in a single line, so that their image formed by a cylindrical lens is a continuous line in which the whole spectrum (0.2-5.1 μm) is concentrated. As a consequence, only the portion of the target shoot by the camera can be illuminated with great efficiency; moreover, the fibres are not equispaced, but positioned in such a way to get uniform intensity on the specimen. A particular illumination system has been designed for this purpose. The target is illuminated with an angle equal to 30° with respect to the normal to the horizontal.

The observed target is positioned on a motorized XYZ translational stage. It is possible to perform an automatized scan of the target by moving the stage step by step in the XY horizontal plane. An image of the slit (9x0.038mm^2) is acquired at each step, obtaining a spectrum for each 0.038x0.038 pixel along the slit. Thus moving the target with respect to the slit at consecutive steps matching the slit width, a number of adjacent slit images are acquired: in this way an hyperspectral cube can be constructed, the number of total steps depending on. The sample to analyse has to be prepared either in powder form or in slab form with at least a plane face. The movement along the Z optical axis is performed during the focus procedure (see section 4). The scattered signal is observed along the normal the horizontal plane (Z-axis). The external optical system is constituted by a flat folding mirror that reflects the scattered light towards an off-axis parabolic mirror. The light from the parabolic mirror enters the TVC through a CaF$_2$ window; inside the chamber a second parabolic mirror deflects the light through another flat folding mirror, and then the light is focused on the entrance slit of the spectrometer. The instrument, like VIR, is based on a spectrometer in Offner configuration (fig.2): generally it is constituted by three spherical concentric elements, that is a primary mirror (concave), a diffraction grating (convex) and a secondary mirror (concave)[5,6]. In this case the primary and secondary mirrors consist of a unique spherical surface.

The light coming from the slit enters the spectrometer, then it is reflected a first time by the spherical mirror on the grating. The diffraction grating (NG5 glass with Al coating) is constituted by two Rowland's circles: a central part with grooves, with about 33% of the total surface, optimized to diffract the VIS light in the range 0.25-1 μm,

and an external corona, of about 67% of the total area, blazed and optimized to diffract IR light in the range 1-5 μm[1]. The light dispersed by the grating is again reflected by the spherical mirror, and finally impinges on the focal planes. The spectral resolution is about 2 nm in the visible and 12 nm in the infrared range.

The spectral range is covered by using two different detectors: a CCD for the visible range and a HgCdTe detector[7,8] for the infrared range. The CCD device has a 1024x1024 pixels matrix, although the sensible part is a window 1024x508 wide. The nominal operating temperature is 155K, at which the corresponding dark current is less than 1electron/sec, that is <1.6x10^{-10} nA. Nevertheless the dark current is very low even at ambient temperature. Each pixel of the CCD is 19x19 μm^2 in size but a spatial binning of 2x2 pixels is performed in order to obtain the same FOV of 38x38 μm^2 for both VIS and IR channels: the spatial resolution thus is of the order of 38 μm. Two bandpass filters are used (250<λ<630 nm and 630<λ<1050 nm) for the visible channel. The Mercury Cadmium Tellurium (HgCdTe) detector is characterized by high quantum efficiency and high electron mobility; the energy band gap and the cut-off wavelength ($\lambda_{cut-off}$) can be tailored by varying the fraction x in the alloy composition Hg$_{1-x}$Cd$_x$Te. The sensor is a matrix of 270x438 pixels with λ_{cut-on}=0.895 μm and $\lambda_{cut-off}$=5.03 μm. The dark current in the IR detector is <10^{-5} nA at 70K. An accumulated charge trans-impedance amplifier (CTIA) allows increasing the sensibility to the low infrared signal; a Correlated Double Sampling (CDS) circuit is then used for the readout of the signal provided by the amplifier. Six bandpass filters are used in order to allow light transmission in six adjacent ranges between 0.9 and 5 μm. Both spectrometer and infrared detector are chilled with liquid nitrogen, at 135K and 77K respectively, in order to minimize dark current due to thermal emission. Moreover inside the TVC ultra-high vacuum is performed (P=10^{-8} mbar) in order to avoid vapour condensation on mechanical and optical parts.
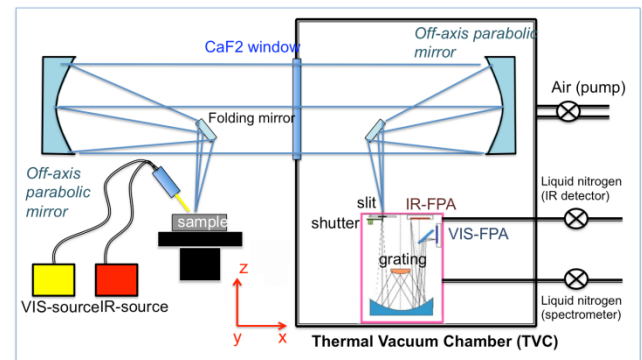

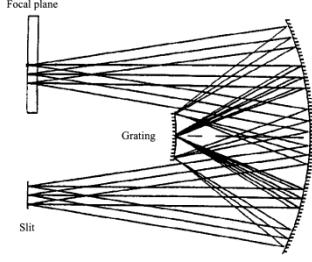Fig.1. Schematic view of the SPIM facility setup.

2

Fig.2. Offner spectrometer configuration adopted for the VIR instrument (De Sanctis et al., 2010).
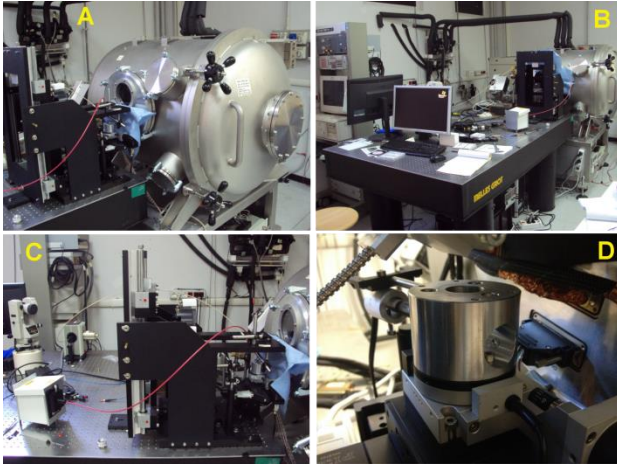

Fig.3. Pictures of the laboratory facility.(A): the Thermal Vacuum Chamber (TVC); (B): the Optical Bench, with EGSE and OGSE; (C): the VIS and IR radiation sources (left) and the external optical layout; on the right the CaF_2 window on the TVC wall is visible; (D): the sample-holder. The HgNe pencil lamp used for transmission measurements is hosted within the cylindrical sample-holder.

3. DATA ACQUISITION AND PRE-PROCESSING

The instrument is an imaging spectrometer: hyperspectral cubes are constructed by performing a scan of the sample in pushbroom mode[9,10]. The scan is performed by moving the sampleholder step by step, using the motorized three axis translational stage, with respect to the spectrometer slit. The movement along the Z (vertical) axis is only used during the focus procedure (see section 4), while during measurement sessions the translation occurs within the XY plane. The scan is performed by translating the stage along the Y direction, that is perpendicularly to the slit X-axis.

Thus matching the amplitude of a step with the width of the slit (i.e. 38 μm) it is possible to cover a desired area on the analyzed sample, by acquiring the signal along the slit at each step and for N consecutive steps. In order to cover an area of 9x10 mm, for example, it is necessary to

perform 10/0.038=263 steps. Finally an hyperspectral cube is obtained with dimensions:

$$Q = b \times s \times l \qquad (1)$$

Where:

- b, bands = spectral dimension (λ, wavelengths)
- s, samples = spatial dimension (Y, along slit)
- l, lines = spatial dimension (X, perpendicular to slit), each line corresponding to an acquisition.

In order to obtain the reflectance spectrum of an analyzed sample, a reference target with standard and certified reflectance is also measured; here we use LabSphere Spectralon targets for the range 0.2-2.5 μm and Infragold for the range 2.5-5.1 μm (see sections 5.3 and 5.4 for characterization). In order to taking into account instrumental and environmental signal that is not directly due to the sample (i.e. the background), a measurements is also performed putting a shutter manually in front of the lamps, thus avoiding of illuminating the sample; this background signal is also present in the sample measurements, and so must be subtracted. The dark current is also measured, closing the automatized shutter in front of the spectrometer slit and acquiring the signal. The reflectance ρ at each wavelength is given by:

$$\rho_\lambda = \frac{(Q_{sample} - S_{bkg-s} - S_{dark-s})/t_{sample}}{(Q_{ref} - S_{bkg-r} - S_{dark-r})/t_{ref}} \qquad (2)$$

in which Q_{sample} and Q_{ref} are the measures of the sample (target to analyze) and the reference respectively. The integration times for the two measures are generally different, tsample and tref; the background and dark current are measured with the same integration times of sample and reference.

The acquisition must be performed separately in the two spectral channels. The measure in the visible is performed keeping only the QTH lamp switched on: this source illuminates in the range 0.2-2.5 μm. The VIS part of the spectrum (0.2-1 μm) is acquired with the CCD, while the NIR part (1-2.5 μm) is acquired with the HgCdTe. The Spectralon is used as reference both for VIS and NIR part. The measure in the infrared is performed keeping only the IR emitter switched on, and acquiring the signal with the HgCdTe in the IR part of the spectrum (2.5-5 μm), where the Infragold is used as reference (fig.4).

Acquisitions in the VIS and IR channels must be performed separately because of the following reason: when the QTH-VIS source is switched on, the signal is too high also in the first half of the IR range and it tends to saturate. Thus, in order to avoid saturation in part of the IR and to optimize the integration time in this spectral range (maximizing the IR signal), the QTH-VIS source is kept

switched off when acquisition in the IR range is performed.

An IDL procedure is used in order to convert the instrument data (*.img*) to cube raw data (*digital numbers*). A second IDL procedure is used to derive calibrated data (*reflectance*) from the raw data.
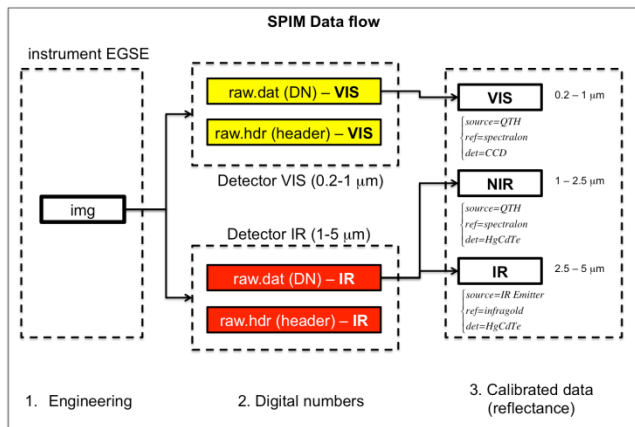

Fig.4. Data flow from the instrument EGSE output up to calibrated data.

4. FOCUS PROCEDURE

The focus procedure allows to determining the exact position (along Z-axis) of the focus of the instrument, so to perform measurements of a target in optimal conditions. This procedure is performed before that a series of measurements sessions is started, once for a day. Doing acquisitions when the target is at the correct focus position, allows to maximize the signal-to-noise ratio.

Here the experimental approach that we followed in the measure procedure is described: the whole procedure is performed while the spectrometer is cooled at its nominal operative temperature, that is T=130-135K.
An HgNe lamp (18 mA power supply; see fig.3D) is used as radiation source, and the measure is made in transmission mode (fig.5): the lamp is put within a cavity inside the cylindrical sample-holder, under the surface corresponding to focal plane.
An external slit (0.5 mm width) is mounted upon the cylindrical sample-holder and it is used in order to limit the field of view. The analysis of a well-defined emission peak in the spectral profile of the lamp radiation allows to determine the position of the focus.
The external slit (S_E) is initially aligned in a direction that is parallel to the spectrometer internal slit (S_I) (fig.5A): this is done by rotating S_E in the XY plane by means of automatized stepper motors, and checking when an acquired frame of the slit (*samples x bands*) shows well-defined peaks. Then, once having verified that the two slits are parallel, the slit S_E is rotated by 90° (fig.5B and 7A).
A sequence of acquisitions is then performed moving the slit vertically along the Z-axis. The typical number N of

steps is about 20, with $\Delta Z=0.1$ mm, and a single VIS acquisition is performed at each step; the supposed focus position is at about half of the vertical survey.

The spectral profile of the HgNe lamp is showed in fig.6. Putting the external slit S_E perpendicularly to the spectrometer slit S_I (fig.7A) it is possible to analyze the spatial profile along X of the slit S_E using few pixels of S_I, and so it is possible to evaluate any small variation of its X-profile (fig.7B).

For each acquisition the horizontal (spatial) profile of the selected emission peak (X-profile) is analyzed (fig.7B). In the ideal case the profile would be rectangular when exactly at focus. Actually the profiles acquired at various heights tend to assume a generic trapezoidal shape, while they tend to be more rectangular when the position approaches the focus. Finally the correct focus position is chosen as the one corresponding to the X-profile that best matches a rectangular shape.
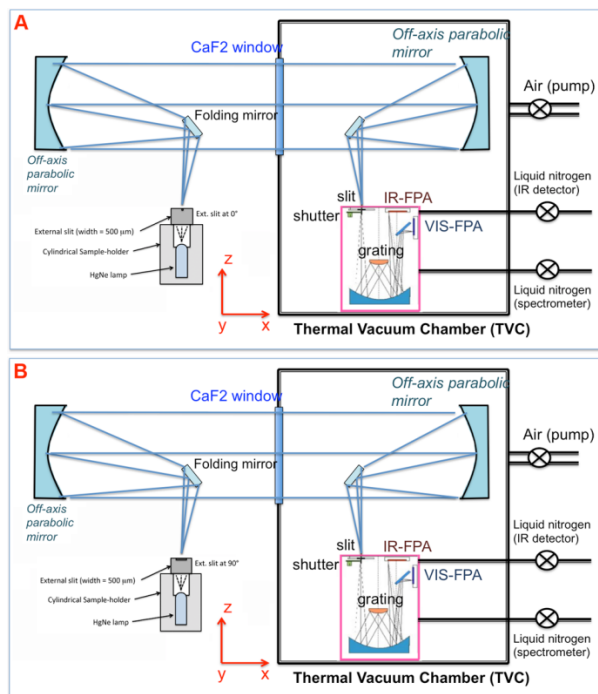

Fig.5. Setup for focus procedure. (A): the external slit is parallel to the spectrometer slit. (B): the external slit is perpendicular to the spectrometer slit.
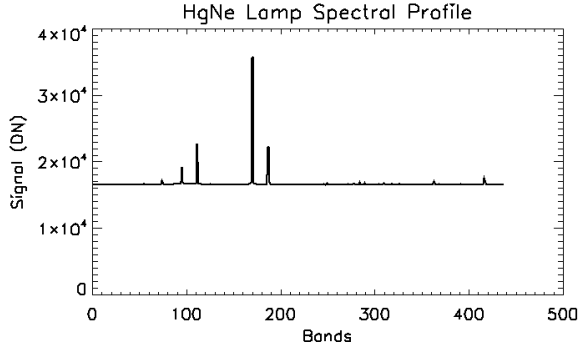
4

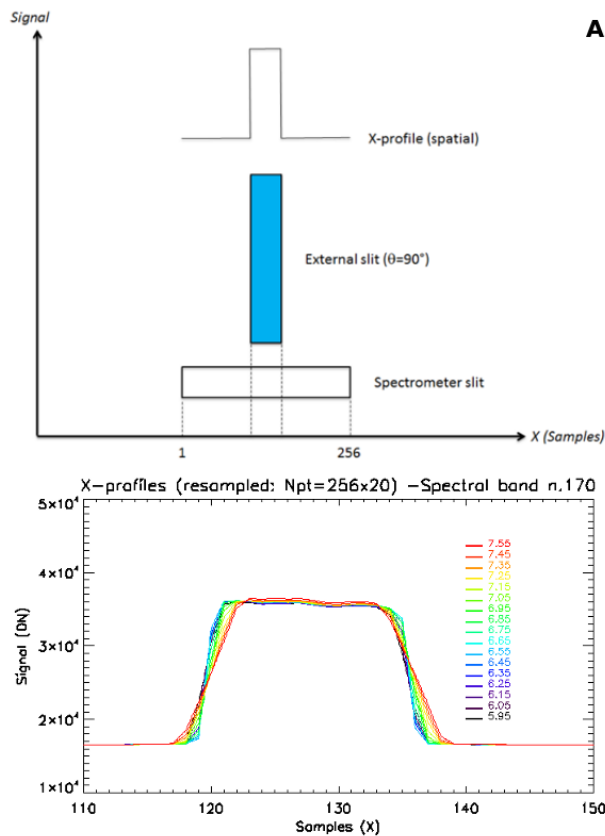Fig.6. Emission spectral profile of the HgNe lamp, used for the focus procedure.

Fig.7. A: relative position of spectrometer slit S_I and external slit S_E (rotated by 90°); in this way only few pixels of the spectrometer slit are illuminated.
B. Visible X-profiles (spatial, i.e. along the spectrometer slit) of an emission peak, acquired along the vertical axis at 18 different heights (from Z=5.95 to Z=7.55), with vertical steps of 0.1 mm. The focus position is roughly at half the height. Profiles far from the focus position tend to assume a trapezoidal form; the correct focus position corresponds to a profile that has a quite regular rectangular shape. The emission line corresponding to band 172 is considered (see fig.6).

5. SPIM CHARACTERIZATION: TESTS

A set of test measurements has been performed in order to characterize the SPIM facility. The very high spatial and spectral resolutions of the instrument force to study and characterize every subsystem separately, in order to measure and quantify the effect of many variables on the final spectra.

The main tests are: light source stability, both for visible and infrared lamps; surface homogeneity of visible (Labsphere © spectralon) and infrared (Infragold) reference targets; detector linearity with different integration times.

5.1 QTH-VIS lamp: stability

The stability of the visible light source has been measured. A LabSphere © spectralon (99% reflectance) has been used as a target: while it was kept fixed on the sampleholder, a series of acquisitions (N=418) were performed on its surface; the QTH lamp was the only light source, thus acquisitions have been obtained in the spectral range 0.22 - 2.5 μm; nevertheless for this test the range 0.22-1.05 μm has been considered.

The integration time of a single acquisition was about Δt_{EXPO}=1s, and the time interval between two consecutive acquisitions was Δt_{INT}=30s; thus the whole measurement time interval was about Δt_{TEST}=3.5h.

Keeping the target fixed, allowed acquiring signal always from the same surface pixels, corresponding to the spectrometer slit (a 256 pixel line); thus the resulting data cube had the following dimensions: X (samples, along slit), Y (lines, along time) and Z (bands, wavelengths).

In this way it has been possible to study the signal on a single pixel in function of the time; because the target was fixed, variations in the pixel signal must be ascribed mainly to fluctuations of the light source irradiation.

All spectra acquired during the Δt_{TEST} and corresponding to a fixed value of sample (s=132, at half the slit length, has been chosen) have been analysed, in particular three different parameters have been measured: the intensity of peak at 0.7 μm (called y_{PEAK1}), the peak at 0.9 μm (y_{PEAK2}), and the slope of the line joining these two peaks (m_{12}-line). A representative spectrum is in fig.8.
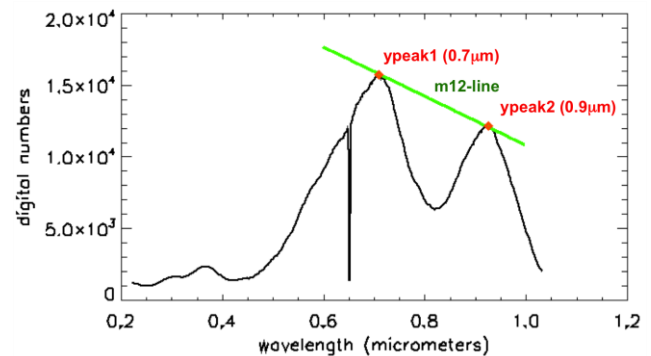

Fig 8. VIS spectrum (DN) of Spectralon 99%. QTH source stability test. The parameters analysed are showed: y_{PK1}, y_{PK2} and relative slope.

For each of the two peaks, the intensity in function of the time has been analysed; as an example, the plot of the y_{PEAK1} intensity is in fig.9. The signal is almost constant within the first 2 hours, and then a series of signal drops appear, with decreasing amplitude and increasing frequency. The intensity data have been linearly fitted; the fit slope (m_1) is a measure of the drift of the signal intensity. Setting y the parameter intensity, the quantity $\Delta y/y_0$ has been measured as a measure of the maximum percent drift, for both 0.7 and 0.9 μm peaks (results are in tab.I), Δy being the maximum intensity variation and y_0 the initial value; the value of the intercept (from the fit result) has been used as y_0. For the 0.7 μm peak we obtain a mean signal variation of about m1=-12.75 DN/h; the corresponding percent variation is $\Delta y_1/y_{0(1)}$=0.28%, where $\Delta y_1 = m_1 * \Delta t$ and Δt=3.48 h.

For the 0.9 μm peak the mean signal variation is m_2=-22.12 DN/h; the percent variation in this case is $\Delta y_2/y_{0(2)}$=0.63%.

The variation of the m_{12}-line parameter with time during Δt_{TEST} has also been evaluated. The values of m_{12} have been plotted in function of time, and a linear fit has been computed: the slope of this fit is itself a measure of the variation of light intensity during Δt_{TEST}. For the slope parameter, we have a mean variation of about m_3=-34.90 DN/h; the percent variation in this case is $\Delta y_3/y_{0(3)}$=0.71%.

The mean fluctuations about the fit values have also been computed for all the analysed parameters; the fluctuations have been determined as follows:

$$\Delta y_{FIT} = \sqrt{\frac{(y_{RAW}-y_{FIT})^2}{y_{FIT}^2}} \times 100 \qquad (3)$$

and then averaged on all values in Δt_{TEST}. The mean fluctuations obtained for the observed parameters are 0.22% (y_{PEAK1}(0.7μm)), 0.28% (y_{PEAK2}(0.9μm)) and 0.95% (m_{12}-line parameter).

In conclusion, both the maximum percent signal drift and the mean signal fluctuation are <1%, during the whole time of measurement (3.5 h). Thus we don't expect any appreciable influence on the signal acquired from samples: the typical duration of a scan is in the range 0.2 – 3.0 h, depending on the form and size of the target (rock powder/slab) and on the integration time.
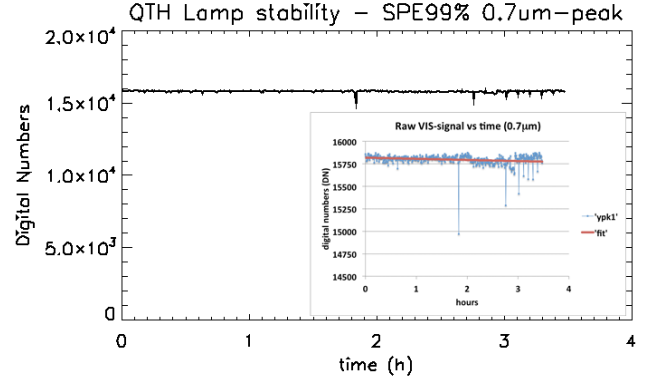

Fig.9. A: y_{PK1} intensity vs time, for a test duration of 3.5 hours. B: the y scale has been restricted (range 14500-16000 DN), and a linear fit has been added.

VIS – QTH source stability parameters			
	y_{PEAK1} (0.7 μm)	y_{PEAK2} (0.9 μm)	m_{12}-line
m	-12.75 DN/h	-22.12 DN/h	-34.90 DN/h
y_0	15818.4 DN	12129.8 DN	-17084.2 DN
$\Delta y/y_0$	-0.28 %	-0.63 %	-0.71 %
$<\Delta y>_{REL}$(%)	0.22 %	0.28 %	0.95 %

Tab.I. VIS source fit parameters: $pk1$, $pk2$, VIS-slope: m=fit slope, y_0=intercept, $\Delta y/y_0$ = max drift, $<\Delta y>_{REL}$ = mean fluctuations.

5.2 IR source: stability

The stability of the IR source has also been evaluated, following the same experimental and analytical approach used for the VIS-lamp characterization.

The infrared reference (LabSphere © INFRAGOLD) has been used as a fixed target; a fixed area of the target, corresponding to the slit area (a 270 pixel line), has been illuminated with the infrared source; a signal acquisition has been registered every Δt_{ACQ} = 25 s, and N_{ACQ} = 200 acquisitions have been carried on during a time interval of about Δt_{TEST} = 1.4 h.

Along the slit line, a central pixel has been chosen (sample = 135), and the spectrum corresponding to this sample has been analysed. For each spectrum two wavelengths have been chosen: λ_1=3.64 μm and λ_2=3.87 μm (see fig.10), and the corresponding raw signal, in digital numbers, has been plotted for all 200 acquisitions, that is in function of time (fig.11).

The choice of these two wavelengths is essentially driven by the fact that they fall out of absorption bands, thus they fall on the continuum. The absorption bands such as those due to H_2O (at 2.8-3.0 μm) or to CO_2 (near 4.2 μm) vary in width and depth during a long time interval (of the order of hours), reflecting the fluctuations of water and carbon dioxide in the laboratory environment. A point located inside or near the wings of such absorption bands would oscillate during time because of these external factors. Points

6

located on the continuum line (such as y_1, y_2 in fig.10) instead will be subject to oscillations due to variations of the radiation source emitted power.
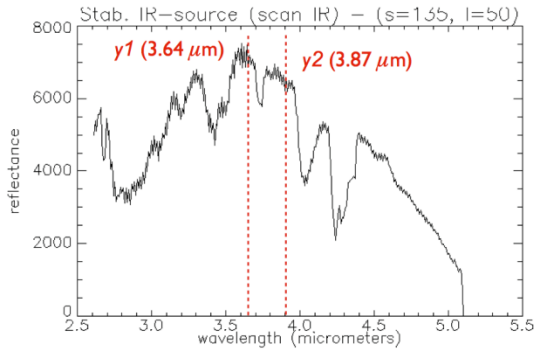

Fig.10. IR spectrum (DN) of Infragold. IR source stability test. The parameters analysed are showed: y_1, y_2.

The plots of y_1 and y_2 raw signal in function of time are showed in fig.11, together with a linear fit. Again the computed slope of the fit can be an indication of the overall variation of the IR signal with time. Here the emitted power appears to be less stable than the VIS case (sec.5.1), and to have an evident drift. If we assume that this drift can be evaluated as the fit slope, then we obtain m_1=-382.62 *DN/h* and m_2=-376.85 *DN/h*. The signal has a maximum decrease of the order of $\Delta y/y_0 \approx$ -7% and the mean fluctuation with respect to the computed fit is about $<\Delta y_{REL}> \approx$ 3%. (see results in tab.II). The whole duration of this test (1.4 h) is greater than the typical duration of an IR measurement session, that is in the range between a few minutes and 1 h.
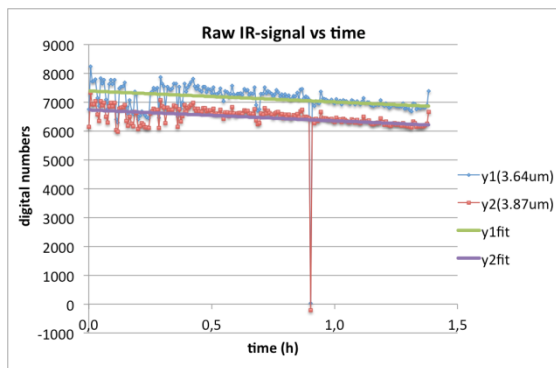

Fig.11. Test of IR-source stability. Analysed parameters are: y_1, raw signal (DN) at λ_1=3.64 μm; y_2, raw signal at λ_1=3.87 μm. Both parameters have been plotted against the time duration of the test.

IR source stability parameters		
	y_1 (3.64 μm)	y_2 (3.87 μm)
m	-382.62 DN/h	-376.85 DN/h
y_0	7386.9 DN	6729.2 DN
$\Delta y/y_0$	-7.16 %	-7.74 %
$<\Delta y>_{REL}$(%)	3.62 %	2.91 %

Tab.II. IR source fit parameters: y_1, y_2, y_0=intercept, $\Delta y/y_0$ = max decrease, $<\Delta y>_{REL}$ = mean fluctuations.

5.3 VIS reference target: surface heterogeneity and roughness

5.3.1 Measure

The surface heterogeneity and roughness of the visible reference target has been characterized. This is a fundamental step in the characterization of the facility: because of the high spatial resolution of the instrument, the measure of the reference target and the subsequent data treatment strongly depends on the knowledge of the surface heterogeneity; then the measure and data reduction of the reference target spectrum obviously influences the final reflectance spectrum of any sample.

A picture with four reference targets (LabSphere Spectralon ©) is showed in figure 12.
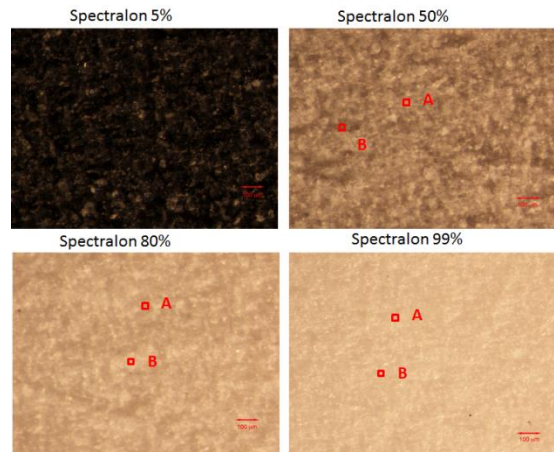

Fig.12. four reference targets (LabSphere spectralon © 5%, 50%, 80% and 99%) photographed with optical microscope. Red squares indicate the spatial spot of SPIM. The surface heterogeneity at μm-scale is evident especially in intermediate targets, such as spectralon 50%: a single spot of SPIM cannot acquire a representative area.

A LabSphere Spectralon © (80% reflectance factor) has been used as a target: a scan consisting of 256 steps (Δx_{STEP}=0.038 mm) has been performed and thus spectra have been acquired from an area of 256x256 pixel (corresponding to an area of 9.7x9.7 mm^2).

Because of the surface heterogeneity of the spectralon, when it is used as a reference in the computation of the reflectance spectrum, a single-pixel spectrum cannot be used: spectra indeed show certain variability from a pixel to another. For that reason an average must be computed over a given number N of acquired reference spectra. The characterization of the surface heterogeneity and roughness of the spectralon will allow estimating the optimal value of N.

Considering a given scan of the target (fig.13), where the X direction is along the spectrometer slit and the Y direction is perpendicular to it and parallel to the target motion, the N reference spectra must be averaged along the Y (lines) direction; indeed we cannot compute the average among spectra along the X (slit) direction, because pixels along X are characterized by different instrument response (fig.13). In fig.14 we can see qualitatively the signal difference between four adjacent pixels.
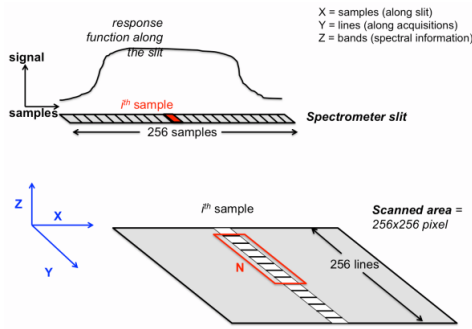

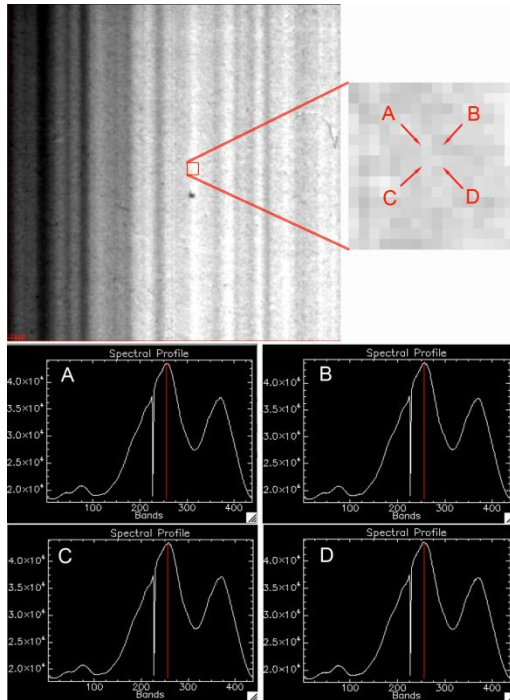Fig.13: VIS-reference target: area scan, heterogeneity, N-pixel-average.

Fig.14: VIS-reference target (Spectralon 80%): scan.

5.3.2   Analysis: single-pixel spectrum

The analysis has been carried on with the following approach. A sample has been fixed along the X direction, namely $s=128$, where the response is maximum. First of all, in order to evaluate the variability of a single spectrum from a pixel to another, the *residue $R_i(\%)$* has been computed between the single spectrum of the ith pixel ($S_i(\lambda)$) and the spectrum averaged on 256 pixels ($<S(\lambda)>$), according to the following relations:

$$\langle S(\lambda) \rangle = \frac{\sum_{i=1}^{256} S_i(\lambda)}{256} \qquad (4)$$

$$\Delta(\lambda)_i^2 = \left(\frac{S_i(\lambda) - \langle S(\lambda) \rangle}{\langle S(\lambda) \rangle} \right)^2 \qquad (5)$$

$$R_i(\%) = \frac{\sum_\lambda |\Delta(\lambda)|}{N_\lambda} \times 100 \qquad (6)$$

where $\Delta_i(\lambda)^2$ is the square deviation. The values $R_i(\%)$ so obtained have been calculated and plotted for all the 256 pixels along the Y direction (fig. 15). The variations are most comprised in the range 1-6%, with a few values near 10%; the mean value is $<R_i(\%)>=2.8\%$.
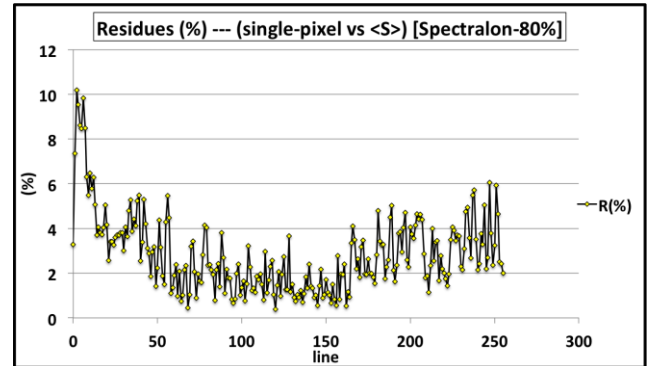

Fig.15. VIS-reference target: residues relative to 1-single-spectrum (S_i) vs. 256-average-spectrum ($<S>$).

5.3.3   Analysis: N-pixel average spectrum

Then different averages have been computed varying the number N of pixels, starting from $N_L=256$ and then reducing N of a half; finally all calculated mean spectra have been compared with the N_L-average-spectrum. In fig. 16 we can see different visible raw spectra, averaged on different numbers N of pixels.
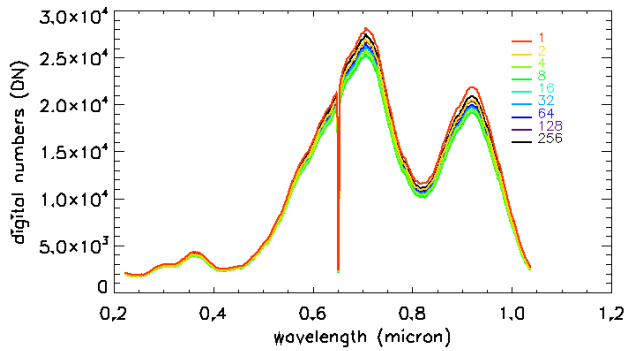
8

Fig. 16. Visible raw spectra of Spectralon, averaged on different number *N* of pixels.

In order to compare the spectra averaged on N pixel with the spectrum , the residues have been computed between $\langle S_N \rangle$ and , where $N=2^k$ spectra and $k=0, \ldots, 7$. The resulting residues have been plotted in fig. 17 (see tab.III): the residue values decrease as the number *N* of pixel increases.
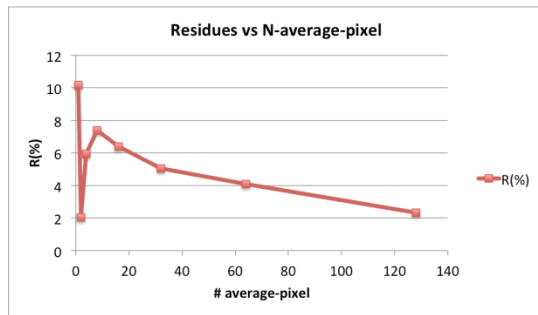

Fig. 17. VIS reference target: residues relative to spectra averaged on different number *N* of pixels vs. 256-average-spectrum.

VIS reference target – residues	
N pixel (average)	R(%) (vs)
1	10.18
2	2.04
4	5.95
8	7.40
16	6.40
32	5.05
64	4.10
128	2.33

Tab.III. VIS reference target: residue values (*N*-pixel average vs. S_{256}).

5.3.4 Analysis: application to band parameters. Sample: pyroxene (enstatite)

Band parameters relative to a pyroxene powder sample (enstatite) have been analysed. For this measure, a 40%-spectralon has been used as reference target, and a scan of 100 steps has been performed on the sample, while a scan of 150 steps has been performed on the reference target, each step being $\Delta x=0.038$ mm.

The reference spectrum has been averaged on *N* pixels, with *N* varying from 150 to 1; an average reflectance spectrum has finally computed for each value of *N*. The average reflectance spectra are showed in fig. 18.
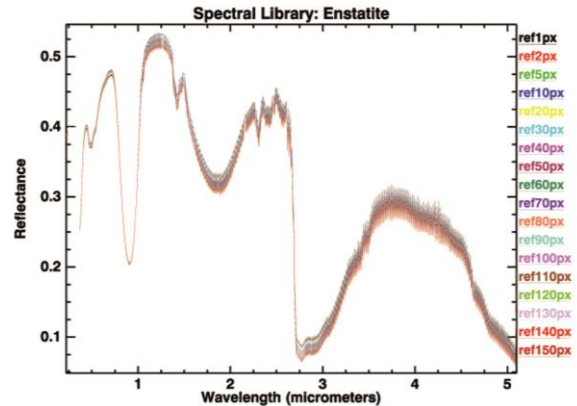

Fig. 18. Enstatite reflectance spectrum, relative to a reference spectrum averaged on *N* pixels (*N* varying from 1 to 150).

In order to estimate the variation of reflectance spectra with respect to the average reference spectrum, mean residues have been computed in two different cases: (i) between each reflectance spectrum (S_i) and the reflectance obtained averaging the spectralon over all 150 pixels (S_{150px}) (fig.19A), (ii) between each reflectance spectrum (S_i) and an average reference spectrum (fig.19B). In the first case the mean residue decreases when the reference spectrum is averaged over the maximum number of pixels (above 100 pixel). In the second case the mean residue is minimized for an average number of pixel of reference (about 60).

Spectral parameters have been determined for the Bands I and II (near 1 and 2 μm respectively), and they are listed in tab.IV. Regarding the Band-I, the minimum, width and center seem do not show any appreciable variation (maximum relative error of 0.0-0.2%). The band depth shows a relative standard deviation of about 0.4% and a maximum relative error of about 1.1%.

Regarding the Band-II, the parameters variations are: the minimum, width and center do not show any appreciable variation (maximum relative error of 0.0-2.0%); the band depth shows a relative standard deviation of about 2% and a maximum relative error of 6.8%.

In any case an optimal number of reference pixel seems to be *N*=150 px: indeed acquiring *N*=150 consecutive steps, each of ΔY=0.038 mm, corresponds to a total area of about 9 mm x 150 x 0.038 mm = 9 x 5.7 mm^2 = 0.5 cm^2, that is representative for all Spectralon surfaces.
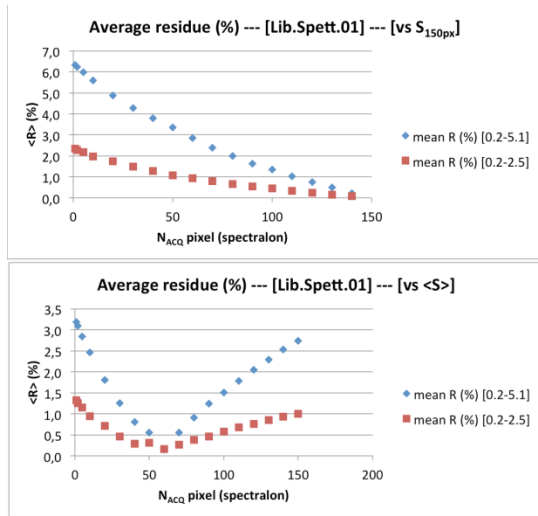
9

Fig.19. A (Left): mean residues computed for each spectrum (S_i) with respect to the spectrum with spectralon averaged over 150 px (S_{150px}). B (Right): mean residues computed with respect to an average spectrum ($<S>$). As expected, in the first case the mean residues are minimized when using the spectrum S_{150px}. In the second case the residues are minimized using a spectrum with spectralon averaged over 60 px.
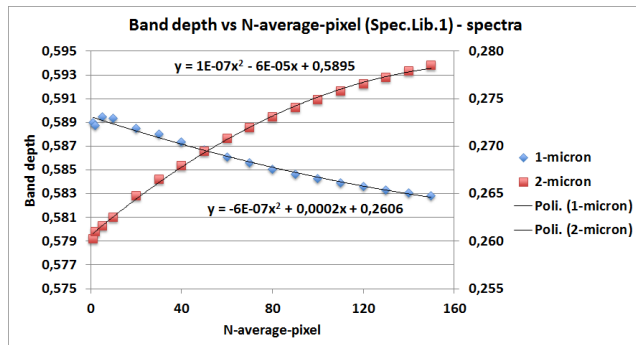

Fig. 20: Enstatite: Band I and II spectral parameters; reference spectrum averaged on variable number N of pixels (0<N<150).

Enstatite – spectral parameters				
Band I (1 μm)				
N-pixel-ref	Minimum (μm)	Center (μm)	Depth	Width (μm)	Depth var. (%)
1	0,908	0,910	0,589	0,215	0,495
2	0,906	0,910	0,589	0,215	0,459
5	0,908	0,910	0,589	0,215	0,573
10	0,906	0,910	0,589	0,215	0,553
20	0,906	0,910	0,589	0,215	0,414
30	0,906	0,910	0,588	0,215	0,328
40	0,906	0,910	0,587	0,215	0,217
50	0,906	0,910	0,587	0,215	0,105
60	0,906	0,910	0,586	0,215	0,005
70	0,906	0,909	0,586	0,215	0,082
80	0,906	0,909	0,585	0,215	0,171
90	0,908	0,909	0,585	0,215	0,246
100	0,908	0,909	0,584	0,215	0,308
110	0,908	0,909	0,584	0,215	0,373
120	0,908	0,909	0,584	0,215	0,425
130	0,908	0,909	0,583	0,215	0,474
140	0,908	0,909	0,583	0,215	0,518
150	0,908	0,909	0,583	0,215	0,553
$<X>$	0,907	0,909	0,586	0,215	
$\sigma_{<X>}$	0,001	0,000	0,002	0,000	
$\sigma_{<X>REL \%}$	0,113	0,028	0,401	0,000	
Band II (2 μm)				
N-pixel-ref	Minimum (μm)	Center (μm)	Depth	Width (μm)	Depth var. (%)
1	1,891	1,863	0,260	0,473	3,708
2	1,891	1,863	0,261	0,473	3,441
5	1,891	1,863	0,262	0,483	3,198
10	1,891	1,863	0,263	0,483	2,875
20	1,891	1,863	0,265	0,483	2,022
30	1,891	1,863	0,267	0,483	1,381
40	1,891	1,863	0,268	0,483	0,851
50	1,891	1,863	0,269	0,483	0,306
60	1,891	1,863	0,271	0,483	0,201
70	1,891	1,863	0,272	0,483	0,632
80	1,891	1,863	0,273	0,483	1,030
90	1,891	1,863	0,274	0,483	1,394
100	1,891	1,863	0,275	0,483	1,719
110	1,891	1,863	0,276	0,483	2,040
120	1,891	1,863	0,277	0,483	2,316
130	1,891	1,863	0,277	0,483	2,584
140	1,891	1,863	0,278	0,483	2,819
150	1,891	1,863	0,279	0,483	3,048
$<X>$	1,891	1,863	0,270	0,481	
$\sigma_{<X>}$	0,000	0,000	0,006	0,003	
$\sigma_{<X>REL \%}$	0,000	0,000	2,310	0,638	

Tab.IV: band I and II (sample Enstatite) spectral parameters, as function of the number of reference pixel.

5.4 IR reference target: surface heterogeneity and roughness

5.4.1   Measure

The surface roughness and heterogeneity of the infrared reference target (the Infragold, LabSphere ©) has also been characterized, in order to evaluate the variability of the signal from a pixel to another. The surface roughness of the reference target clearly influences the reflectance value obtained measuring a rock or mineral.

The experimental approach is similar to that described in the section 5.3.1. The target (Infragold) has been illuminated with the IR radiation source, while being moved along the Y-axis (fig. 21) for N=270 steps, each step equal to 0.038 mm; in the case of the IR detector the slit is subdivided into 270 pixels, thus the whole scan of the Infragold consists of 270x270 pixel (corresponding to an area of about 10.3x10.3 mm^2, see fig. 22). In fig. 22 we can qualitatively realize the surface heterogeneity of this reference target just looking at the four different raw spectra acquired in four adjacent pixels. If we compare this figure with that relative to the Spectralon (fig. 14) we can immediately realize that the Infragold is characterized by a surface heterogeneity much greater than the one of the Spectralon; thus we can anticipate that in the IR case it will be necessary to average the reference target acquisitions over a greater number N of pixels.
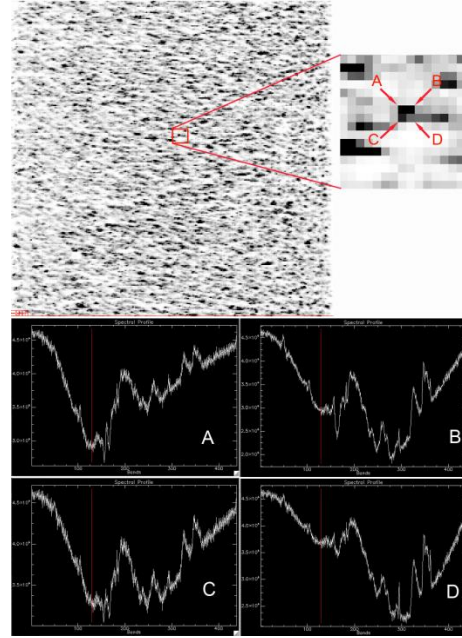

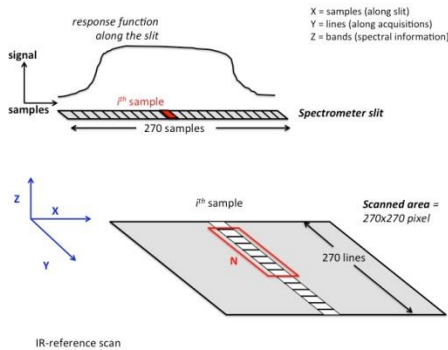Fig. 22. IR-reference target (Infragold): scan.

Fig. 21. IR-reference target: area scan, heterogeneity, N-pixel-average.

5.4.2 Analysis: single pixel spectrum

The analysis has been carried out following the same approach as in sec.5.3.2. A sample has been fixed along the X direction at half the slit, namely s=135, where the response is maximum.

In order to evaluate the variability of a single spectrum from a pixel to another, the residue $R_i(\%)$ has been computed between the single spectrum of the ith pixel ($S_i(\lambda)$) and the spectrum averaged on 270 pixels ($<S(\lambda)>$), according to the relations in eq.4, 5 and 6.

The values $R_i(\%)$ so obtained have been calculated and plotted for all the 270 pixels along the Y direction (fig. 23). Most of the residue values are comprised in the range 10-100%, with a mean value of about $<R_i(\%)>$=63%.
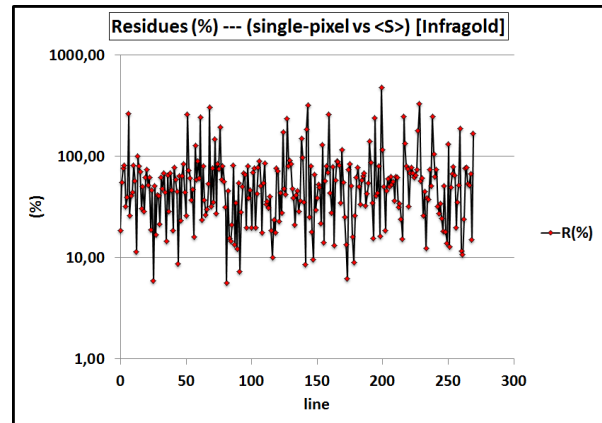

Fig. 23. IR-reference target: residues relative to 1-single-spectrum (S_i) vs. 270-average-spectrum ($<S>$).

11

5.4.3   Analysis: N-pixel average spectrum

As for the visible case (sec.5.3.3), different averages have been computed varying the number N of pixels, starting from N_L=270 and then reducing N of about a half; finally all calculated mean spectra have been compared with the N_L-average-spectrum. Infragold raw spectra averaged on different N of pixels are in fig. 24. The residues have been computed between <S_N> and , where N=270, 136, 68, …,1 spectra, in order to compare the spectra averaged on N pixels with the spectrum . The residues have been plotted in fig. 25 (values in tab.V): the residue values decrease as the number N of pixel increases, thus for example we obtain a residue of 10% if we average the reference spectra over about 100 pixels.
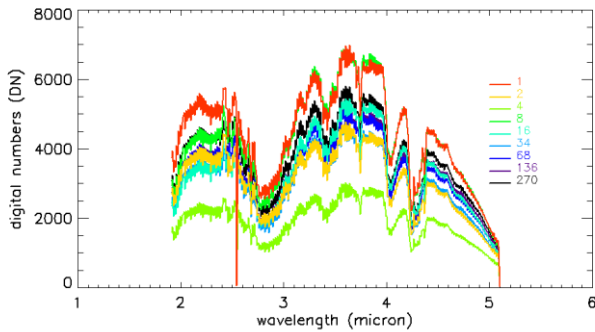

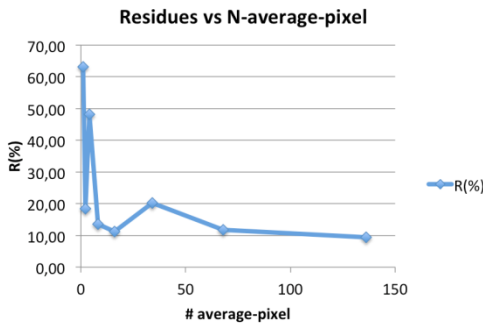Fig. 24. IR raw spectra of Infragold, averaged on different number N of pixels.

Fig. 25. IR reference target: residues relative to spectra averaged on different number N of pixels vs. 270-average-spectrum.

IR reference target – residues	
N pixel (average)	R(%) (vs)
1	63.05
2	18.54
4	48.26
8	13.62
16	11.25
34	20.16
68	11.82
136	9.42

Tab.V. IR reference target: residue values (N-pixel average vs. S270).

5.5 DETECTOR LINEARITY WITH Δt_{EXPO}: VIS CASE

The linearity of response of the visible detector (CCD) has been investigated. This has been carried out by observing the same target at different integration times and then evaluating how the signal increased. Two spectralon references have been used as targets (80% and 99%). In both cases the target has been kept fixed with respect to the spectrometer slit: a fixed area, corresponding to the slit, has been observed varying the integration time with steps of Δt_{VIS}=500 ms. Six different integration times have been used in the range from t_{EXPO}=0.5 s to t_{EXPO}=3.0 s, performing one acquisition and then varying the integration time by Δt_{VIS}=500 ms. This sequence of six acquisitions has been repeated five times for both targets.

The analysis of measurements has been carried out in the following way. For each target the raw measured signals have been considered, without performing any signal processing or manipulation (fig. 26).
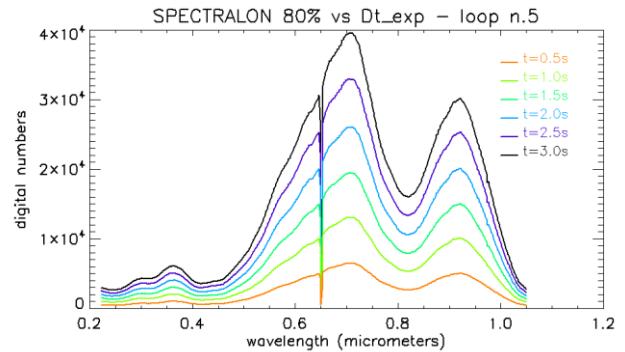

Fig. 26. Acquisitions at 7 different integration times. From orange to black curve, the $t_{EXPO\text{-}VIS}$ increases linearly from 0.5 to 3.0 s.

For each acquired signal the maximum value has been selected (peak at 0.7 μm), and then all these values have been plotted versus the corresponding integration time; this evaluation has been repeated for the 5 sequences of measurements (fig. 27). The perfect linearity of the detector response in this range is evident in both cases.
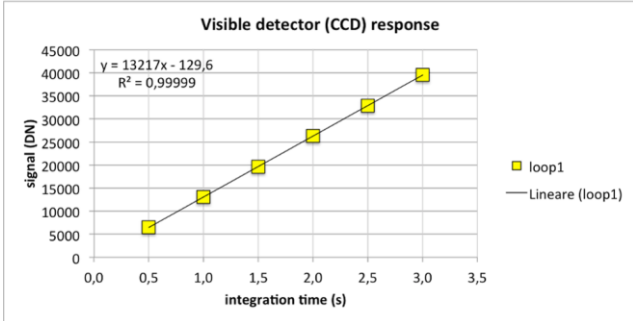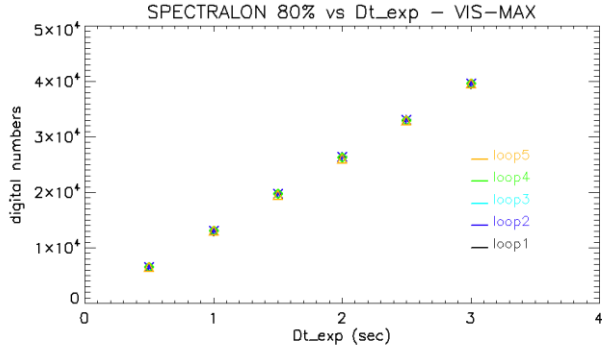
Fig.28. Acquisitions at 8 different integration times. From orange to black curve, the $t_{EXPO-IR}$ increases linearly from 0.04 to 0.18 s, with increments of Δt=0.02 s. The signal readout in the IR detector is inverted with respect to the CCD detector, so the lower spectra (towards black) correspond to higher signal. The saturation occurs at 9x103 DN.

The raw and unprocessed signals have been analysed in a similar way as for the visible case. In the infrared case three different signal levels have been evaluated (corresponding at the wavelengths λ_1=2.11μm, λ_2=3.7μm and λ_3=3.9μm), in order to select points well outside the absorption bands. The signal level corresponding to λ_1=2.11μm has been plotted versus the integration time, for all the five sequences (fig. 29). The linear response of the infrared detector at different integration times, in this range, is evident.

Fig.27. Left: maximum signal level (peak at 0.7 μm) plotted versus the integration time, for spectralon 80%. Right: a linear fit has been computed for data of the loop 1.

5.6 DETECTOR LINEARITY WITH Δt_{EXPO}: IR CASE

A similar evaluation has been carried out concerning the infrared detector response (HgCdTe). A reference standard (LabSphere Spectralon 40%) has been used as a target. During the observation the target has been kept in a fixed position. The experimental procedure is the same as described in the previous section. Eight different integration times have been used in the range 0.04-0.18 s (with steps of Δt_{IR}=20 ms); the raw profiles are plotted in fig. 28. Raw data from infrared detector have signs inverted with respect to the data from CCD: thus lower values of digital numbers correspond to higher signal, and are obtained with longer exposition times. The detector saturation occurs at about 9000 DN.
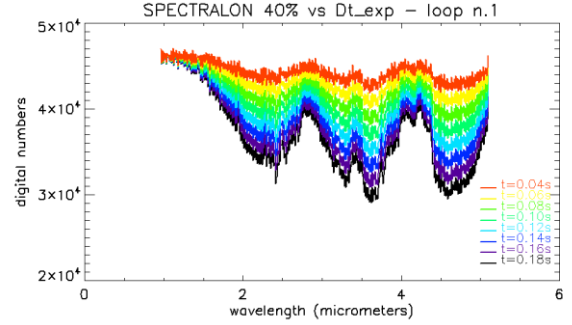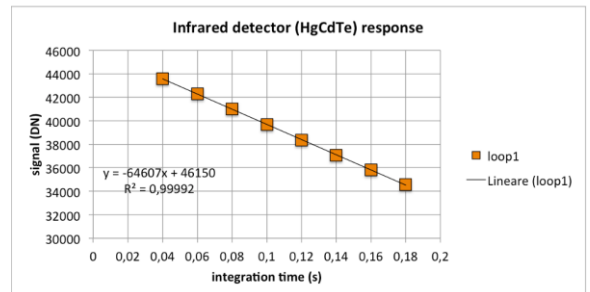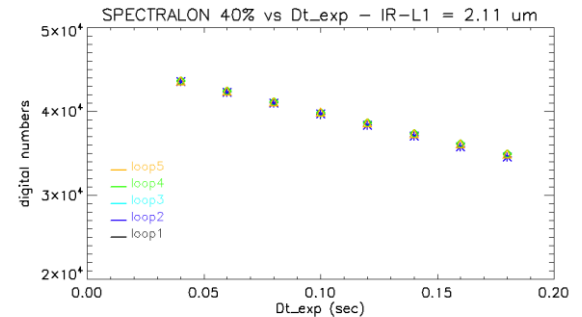

Fig.29. Left: IR signal level (peak at 2.11 μm) plotted versus the integration time, for spectralon 40%. Lower values of digital numbers correspond to higher signal (the signal readout in the IR detector is inverted with respect to CCD detector), obtained with longer exposition times. Right: a linear fit has been computed for data of the loop 1.

13

5.7 NOISE REDUCTION

5.7.1 Vertical Striping

Vertical striping occurs mostly in the IR range of spectrum 2.5-5 μm. Vertical striping arises in a large number of multidetector pushbroom imaging instruments. It is a spatially and spectrally coherent noise produced by sensitivity variations between neighboring elements of detectors[11].

Many destriping methods have been proposed in the literature. The methodology used here[12] assumes that the noise contribution changes from one pixel to another in the across-scan direction and it has thus a high spatial frequency; the noise contribution from the signal of the target has instead a lower spatial frequency, and so they can be theoretically separated.

First, the methodology estimates the high frequency noise by calculating the average above all the lines for each sample (column of the image). The matrix resulting from lines averaging is filtered by LPF (low pass filter) to eliminate the high frequency noise. Then the procedure calculates the ratio between unfiltered and filtered matrix in order to extract the correction matrix that will be applied line by line[12].

The algorithm assumes a general homogeneity of the signal response of the scene. Nevertheless, in some cases in which the average of a column is strongly influenced by great signal variations, the correction effect would alter the signal. To avoid these "overcorrection" effects the possibility was implemented to set a limit value for the correction of the signal.

The effectiveness of the procedure for vertical striping correction has been verified checking that the mean value of the difference between corrected data and original data is negligible, that spatial features are preserved after the correction; that the procedure itself does not introduce artifacts.
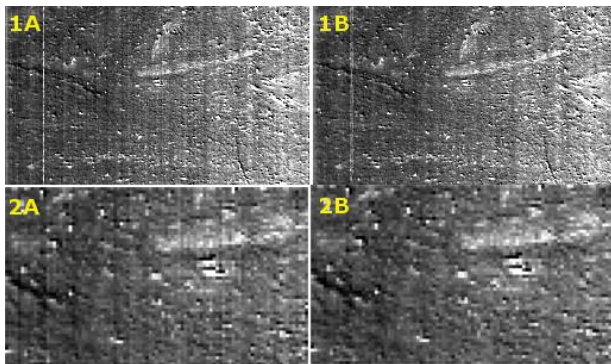

Fig.30. Example of application of the destriping algorithm to a scan. The sample is a volcanic rock slab. 1A: monochromatic image acquired with SPIM, corresponding to the whole scan (λ=4.17 μm). The vertical stripes are evident. 1B: the destriping algorithm has been applied to the same

image. A 3x1 pixel box has been used in order to smooth. 2A: zoom of the raw image. 2B: zoom of the destriped image.
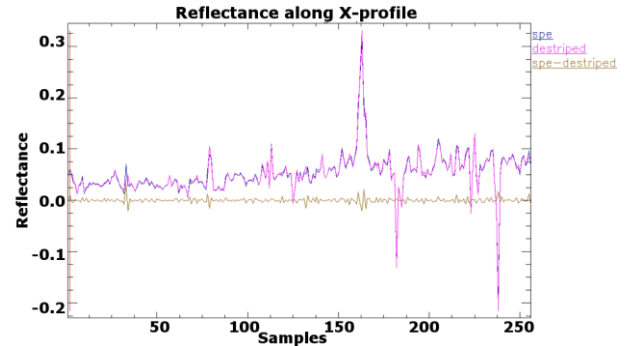

Fig.31. Blue curve: X-profile of the image. Purple curve: X-profile of the destriped image. The fluctuations along the samples decrease. Ochre curve: difference between the two X-profiles.

5.7.2 Spectral Spiking

A spectral spike is characterized by an increased amplitude of the signal in corrispondence of a single band or a couple of bands. Since spikes can lead to spectral misidentification, an algorithm was implemented for spiking correction in SPIM spectra, that consists in spikes detection. The detection consists on checking the signal difference between the signal of one band and the two neighbouring. Where signal difference is greater than an edge value (percent of signal of neighbouring sample), spike is detected and the correspondent value is then removed from the spectrum.

If we call y_j the signal corresponding to the jth band, the algorithm iteratively checks if the following two conditions are simultaneously verified:

$$\begin{cases} |y_j - y_{j-1}| > t \times y_{j-1} \\ |y_j - y_{j+1}| > t \times y_{j+1} \end{cases}$$

Here the parameter t is a percent threshold, generally set at about 20%. If both conditions are verified, the spike y_j is identified. The applied correction consists of a straight line traced between y_{j-1} and y_{j+1}. In fig.32 an example is showed of a spectrum with a spike, and the same spectrum after spike removal.
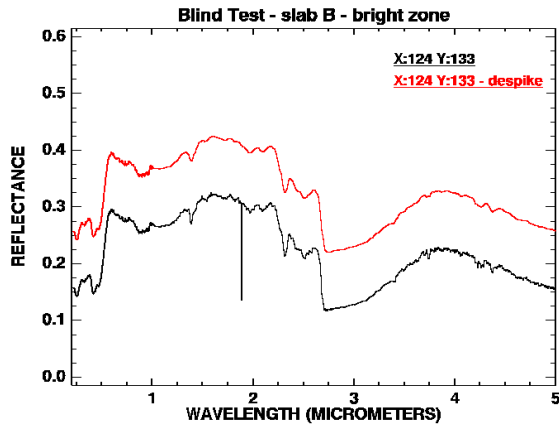
Fig.32. Example of despiking. Top: spectrum of volcanic rock slab, relative to a single pixel, with a spike at about 1.9 μm. Bottom: the same spectrum after the despiking algorithm has been applied.

5.7.3   Banding

Vertical aperiodic banding occurs as dark-clear banding in SPIM data and is evident on reference targets used for reflectance calibration (example in fig.33). The noise occurs at fixed positions. It is due to not perfect profile of the response along the slit. A quantitative estimation of signal intensity in the raw data affected by banding was computed: (i) computing a 2nd order polynomial fit of X-profiles (samples); (ii) determining the fluctuations between raw data and the fit. An example is showed in fig.34. The targets used were Spe10, Spe40, Spe50, Spe99 for measurements in visible and near infrared range and Infragold target for infrared range. In the NIR range, the algorithm removes signal spikes before calculating the curve fit. As a result, the variation in signal intensity ranges about 0-7% for visible range and rise up to 12% in peripheral samples (first and last ten). In the NIR range the signal oscillates between 0 and 10% and rise up to 25% in the first and last ten samples. In IR range, the variation stands between 0-5% and rise up to 7% in the peripheral samples.
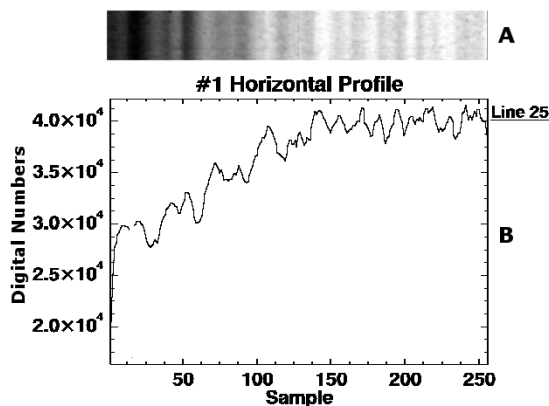

Fig.33. A: scan of spectralon 99% (monochromatic image). The alternation of darker and lighter vertical zones constitutes the banding. B: X (horizontal) profile. It is possible to note the signal fluctuation.
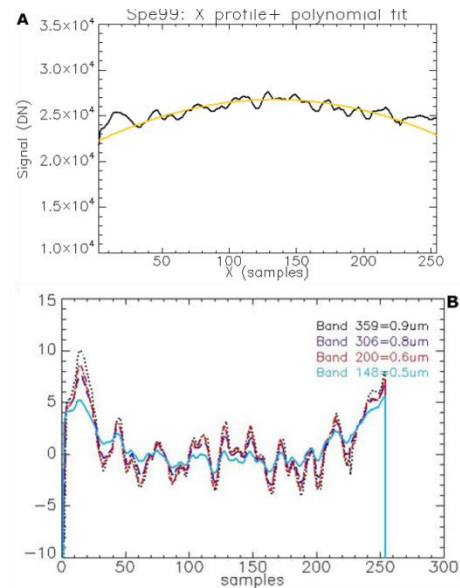

Fig.34. A: X profile and polynomial fit (2° order). B: percent residues computed between X-profile and polynomial fit; this calculation has been done for 4 different wavelengths.

6.   CONCLUSIONS

The visible and infrared imaging spectrometer SPIM has been characterized. A series of laboratory tests have been performed on instrument subsystems: (i) measure of the stability of visible and infrared radiation sources; (ii) analyses of the surface heterogeneity of visible and infrared reference targets; (iii) measure of the linearity of CCD and HgCdTe detectors.

The VIS radiation source has proved to be stable within a timescale of about 3 h, with a mean fluctuation <1% and a maximum signal decrease of about -0.7% within the observed timescale. The IR source is stable within 1.5 h, with a mean fluctuation <3% and a maximum signal decrease of about -7.7%.

Analyses of surface heterogeneity of the visible reference target (LabSphere Spectralon 80%) has been performed: the difference in raw spectra (estimated as residue) from a pixel to another is in the range 1-10%, with an average value of about 3%. In the computing of the reflectance spectrum, the spatial average (in the direction orthogonal to the spectrometer slit) over at least 100 pixels of Spectralon leads to a variation in reflectance spectra of the order of <3%.

The reference target used for the IR (LabSphere Infragold) shows a greater surface heterogeneity; the residues for raw spectra from pixel to pixel are in the range 10-100%, with

15

a mean value of about 63%. In order to obtain a variability of <10% in reflectance spectra, a spatial average over at least 150 pixels on the Infragold must be performed.

Detector response measurements have showed that there is a good linearity vs. the integration time both for the CCD (range 0.5 – 3.0 s for the analyzed targets, Spectralon 80% and 99%) and the HgCdTe (range 0.04 – 0.18 s for the Spectralon 40%).

Instrumental imaging artifacts have also been investigated, in order to take them into account during the analysis of spectral data. Identified artifacts are essentially of three types: (i) striping, (ii) banding and (iii) spectral spiking. Algorithms have been implemented in order to correct both striping and spectral spiking. Banding is currently not corrected: if we consider the 240 central pixels along the slit, the signal variation is <7% in the VIS range (0.2 – 1.0 μm), <10% in the NIR range (1.0 – 2.5 μm) and <5% in the IR range (2.5 – 5.1 μm).

This facility can play a fundamental role in the laboratory investigation of terrestrial (minerals, rocks) and extraterrestrial (meteorites, micro-meteorites) samples as well as for the validation of remote-sensing/in situ planetary future data; this can be done thanks to its peculiar characteristics: (i) high spectral (2-10 nm) resolution, (ii) high spatial (38 μm) resolution, (iii) its wide and continuous spectral range (0.2-5.1 μm), and (iv) to the fact that both samples in the form of slab and powder can be analyzed.

With this aim we are proceeding with the acquisition of spectral data about rock-forming minerals, various types of rocks and meteorites: these data will build a very powerful and useful high resolution spectral database.

ACKNOWLEDGEMENTS

REFERENCES

[1]De Sanctis M.C. et al., The VIR Spectrometer, Space Sci. Rev. 163:329–369, DOI 10.1007/s11214-010-9668-5, (2011)

[2]Russell, C.T. et al.: Dawn: A journey in space and time, Planetary and Space Science, 52, pp 465–489, (2004)

[3]Vago, J.L., et al.: ExoMars, ESA's next step in Mars exploration. ESA Bull. Mag. 155, 12–23, (2013)

[4]Coradini A. et al., Laboratory measurements in support of the DAWN mission: the Spectral IMaging (SPIM) facility, EPSC Abstracts, Vol.6, EPSC-DPS2011-1043 (2011)

[5]Prieto-Blanco X. et al.: Analytical design of an Offner imaging spectrometer, Optics Express vol.14, N.20, (2006)

[6]Gonzalez-Nunez H. et al.: Design, calibration and assembly of an Offner imaging spectrometer, IOP Publishing, Journal of Physics: Conference series 274, doi:10.1088/1742-6596/274/1/012106, (2011)

[7]Norton P.: HgCdTe infrared detectors, Opto-electronics Review, 10(3), 159-174, (2002)

[8]Rogalski A.: HgCdTe infrared detector material: history, status and outlook, Rep. Prog. Phys. 68, 2267–2336, doi:10.1088/0034-4885/68/10/R01, (2005)

[9]Melchiorri R.: Calibrazione e preparazione alla spettroscopia ad immagine, PhD Thesis, Università Degli Studi di Roma "La Sapienza" and Università di Parigi "Denis Diderot", XVII ciclo, (2004)

[10]Filacchione G.: Calibrazioni A Terra E Prestazioni In Volo Di Spettrometri Ad Immagine Nel Visibile E Nel Vicino Infrarosso Per L'esplorazione Planetaria, PhD Thesis, Università Degli Studi Di Napoli "Federico II", XIX ciclo, (2006)

[11]Gómez-Chova L., Alonso L., Guanter L., Camps-Valls G., Calpe J. and Moreno J.- Correction of systematic spatial noise in push-broom hyperspectral sensors: application to CHRIS /PROBA images - Applied Optics, Vol. 47, Issue 28, pp. F46-F60, (2008)

[12]Barducci et al., Chris-Proba Performance Evaluation: Signal-To-Noise Ratio, Instrument Efficiency And Data Quality From Acquisitions Over San Rossore (Italy) Test Site, Proc. of the 3rd ESA CHRIS/Proba Workshop, 21–23 March, ESRIN, Frascati, Italy, (ESA SP-593, June 2005), (2005)